DOI: 10.1002/ejic.200701104

Syntheses, Structures, and Electrochemical and Magnetic Properties of Rectangular Heterobimetallic Clusters Based on Tricyanometallic Building Blocks

Cai-Feng Wang,[a] Wei Liu,[a] You Song,[a] Xin-Hui Zhou,[a] Jing-Lin Zuo,*[a] and Xiao-Zeng You[a]

Keywords: Cyanometalates / Crystal structures / Magnetic properties / Single-molecule magnets / Polynuclear complexes

Three tricyanometalate precursors, $(Bu_4N)[(PhTp)Fe(CN)_3]\cdot H_2O$ (**1**), $(Bu_4N)[(MeTp)Fe(CN)_3]$ (**2**), and $(Bu_4N)[(i\text{BuTp})Fe(CN)_3]$ (**3**) [Bu_4N^+ = tetrabutylammonium cation; PhTp = tris(pyrazolyl)phenylborate; MeTp = methyltris(pyrazolyl)borate; *i*BuTp = 2-methylpropyltris(pyrazolyl)borate], were successfully synthesized. By using **1**–**3** as building blocks, four rectangular clusters, $[(PhTp)Fe(CN)_3Cu(bpy)(H_2O)(ClO_4)]_2\cdot 2H_2O$ (**4**; bpy = 2,2′-bipyridine), $[(PhTp)Fe(CN)_3Ni(tren)]_2(ClO_4)_2$ [**5**; tren = tris(2-amino)ethylamine], $[(MeTp)Fe(CN)_3Ni(tren)]_2(ClO_4)_2\cdot 2H_2O$ (**6**), and $[(i\text{BuTp})Fe(CN)_3Ni(tren)]_2(ClO_4)_2\cdot 2H_2O\cdot 2CH_3OH$ (**7**), were prepared in parallel and structurally characterized. All clusters show similar square structures, where Fe^{III} and M^{II} ($M = Cu^{II}$ or Ni^{II}) ions are alternatively located on the rectangle corners. The cyclic voltammograms of $Fe^{III}_2Ni^{II}_2$ clusters **5**–**7** reveal two quasi-reversible iron-centered reduction processes and two quasi-reversible nickel-centered oxidation processes. Magnetic studies show intramolecular ferromagnetic coupling and appreciable magnetic anisotropy in clusters **4**–**7**. Complexes **5**–**7** show obvious frequency dependence in the alternating current magnetic susceptibility data, which indicates single-molecule magnet behavior with preexponential factors of $\tau_0 = 4.5\times10^{-8}$ s (**5**), 6.1×10^{-8} s (**6**), and 5.0×10^{-8} s (**7**) and the effective spin-reversal barriers of U_{eff} = 17.5 K (**5**), 20.6 K (**6**), and 20.8 K (**7**).

Introduction

Research on single-molecule magnets (SMMs) has attracted increasing interest in the field of molecular magnetism.[1,2] Below the blocking temperature, these kinds of molecules exhibit slow relaxation of the magnetization induced by the combined effect of a high-spin ground state (S) and a negative uniaxial anisotropy ($D < 0$), which generates an energy barrier (U) between spin-up and spin-down states with upper limits given by $|D|S^2$ or $|D|(S^2–1/4)$ for integer and half-integer spins, respectively. This bistability makes them potentially applicable in high-density data storage and quantum computing.[3] Recently, considerable effort has been devoted to metal–cyanide compounds as fascinating candidates for the preparation of high-spin anisotropic clusters,[2b,4–17] and some of them behave as SMMs.[14–17] With use of cyanide as a bridging ligand, the topological structures and the nature of the magnetic exchange interactions (ferromagnetic or antiferromagnetic) in the resulting cluster may be controlled and predicted to some extent.[4,18] One effective approach to synthesize cyano-bridged SMMs refers to employment of modified cyanometalates $[M(L)_y(CN)_x]^{(x-m)-}$ (L = Me_3tacn, Tp, bipy, etc.) as building blocks toward fully solvated transition-metal ions or coordinatively unsaturated metal complexes.[2b,15–17] Here, organic blocking ligands can be utilized to direct the assembly of specific structures, wherein variation of the metal ions can provide adjustability to both spin state and magnetic anisotropy.

Very recently, those precursors related with tris(pyrazolyl)borate iron(III) tricyanide have been widely investigated.[8–12,16,17,19] The low-spin Fe^{III} ion in these precursors possesses unquenched first-order orbital angular momenta, which gives rise to significant single-ion magnetic anisotropy.[20] In our previous work, with the building block $[(Tp)Fe^{III}(CN)_3]^-$ [Tp = tris(pyrazolyl)hydroborate], a series of cyano-bridged heterobimetallic complexes were prepared with different magnetic properties from ferromagnetism and metamagnetism to single-molecule magnetism, single-chain magnetism, and spin-glass behavior.[9,16,19] It is believed that the main anisotropy resource lies on the orbit contribution of the Fe^{III} centers. We also observed that intermolecular interaction generally has some negative impact on SMM or single-chain magnet (SCM) behavior. The enhancement in the steric effect by introducing steric

[a] Coordination Chemistry Institute and the State Key Laboratory of Coordination Chemistry, School of Chemistry and Chemical Engineering, Nanjing University,
Nanjing 210093, P. R. China
Fax: +86-25-83314502
E-mail: zuojl@nju.edu.cn

Supporting information for this article is available on the WWW under http://www.eurjic.org or from the author.

groups on B atoms in Tp is one of possible approaches to decrease the intermolecular interaction, and this imposes no influence on the construction of the multinuclear clusters. With this strategy in mind, we synthesized three new building blocks, $(Bu_4N)[(L)Fe(CN)_3]\cdot nH_2O$ [Bu_4N^+ = tetrabutylammonium cation; L = tris(pyrazolyl)phenylborate (PhTp), n = 1, **1**; L = methyltris(pyrazolyl)borate (MeTp), n = 0, **2**; L = 2-methylpropyltris(pyrazolyl)borate (*i*BuTp), n = 0, **3**]. Their reaction with some partially blocked salts afforded four heterobimetallic rectangular clusters, $[(PhTp)Fe(CN)_3Cu(bpy)(H_2O)(ClO_4)]_2\cdot 2H_2O$ (**4**; bpy = 2,2′-bipyridine), $[(PhTp)Fe(CN)_3Ni(tren)]_2(ClO_4)_2$ [**5**; tren = tris(2-amino)ethylamine], $[(MeTp)Fe(CN)_3Ni(tren)]_2(ClO_4)_2\cdot 2H_2O$ (**6**), and $[(i\text{BuTp})Fe(CN)_3Ni(tren)]_2(ClO_4)_2\cdot 2H_2O\cdot$

Table 1. Selected bond lengths [Å] and angles [°] for complexes **1**–**3**.

1							
Fe1–C1	1.914(7)	Fe1–C2	1.912(7)	Fe1–C3	1.901(6)	Fe1–N4	1.947(4)
Fe1–N6	1.987(4)	Fe1–N8	1.966(4)	C1–N1	1.154(7)	C2–N2	1.149(7)
C2–Fe1–C1	88.6(3)	C3–Fe1–C1	88.9(2)	C3–Fe1–C2	88.6(2)	N4–Fe1–N6	86.93(18)
N4–Fe1–N8	87.14(18)	N8–Fe1–N6	88.36(18)	N1–C1–Fe1	177.4(6)	N2–C2–Fe1	177.7(6)
N3–C3–Fe1	179.1(5)						
2							
Fe1–C1	1.909(5)	Fe1–C2	1.913(6)	Fe1–C3	1.915(5)	Fe1–N4	1.980(4)
Fe1–N6	1.970(4)	Fe1–N8	1.958(4)	C1–N1	1.154(5)	C2–N2	1.159(6)
C2–Fe1–C1	89.0(2)	C3–Fe1–C1	89.55(19)	C3–Fe1–C2	85.8(2)	N4–Fe1–N6	87.16(16)
N4–Fe1–N8	88.30(18)	N8–Fe1–N6	87.64(18)	N1–C1–Fe1	178.2(4)	N2–C2–Fe1	175.8(5)
N3–C3–Fe1	177.7(5)						
3							
Fe1–C1	1.929(3)	Fe1–C2	1.928(3)	Fe1–C3	1.920(3)	Fe1–N4	1.9702(18)
Fe1–N6	1.9750(19)	Fe1–N8	1.965(2)	C1–N1	1.141(3)	C2–N2	1.142(3)
C2–Fe1–C1	88.98(10)	C3–Fe1–C1	89.77(10)	C3–Fe1–C2	86.18(11)	N4–Fe1–N6	87.26(8)
N4–Fe1–N8	87.77(8)	N8–Fe1–N6	88.24(8)	N1–C1–Fe1	176.3(3)	N2–C2–Fe1	179.4(3)
N3–C3–Fe1	174.9(2)						

Table 2. Selected bond lengths [Å] and angles [°] for complexes **4**–**7**.

4							
Fe1–C16	1.919(5)	Fe1–C17	1.931(5)	Fe1–C18[a]	1.921(4)	Fe1–N5	1.948(3)
Fe1–N1	1.961(3)	Fe1–N3	1.969(3)	Cu1–N9	1.948(4)	Cu1–N8	1.956(4)
Cu1–N10	1.997(4)	Cu1–N11	2.016(4)	Cu1–O1	2.370(3)	Cu1–O3	2.391(3)
C18[a]–Fe1–C17	86.75(17)	N9–Cu1–N8	92.18(15)	N8–C17–Fe1	176.6(4)	N9–C18–Fe1[a]	177.8(4)
C17–N8–Cu1	174.8(4)	C18–N9–Cu1	176.6(4)	N10–Cu1–N11	80.05(16)	N9–Cu1–N10	170.99(16)
O1–Cu1–O3	169.63(10)	N9–Cu1–O1	94.41(14)	N9–Cu1–O3	93.83(13)		
5							
Fe1–C1	1.925(5)	Fe1–C2	1.923(5)	Fe1–C3	1.914(5)	Fe1–N5	1.948(3)
Fe1–N7	1.966(4)	Fe1–N9	1.968(4)	Ni1–N2	2.053(4)	Ni1–N3	2.098(4)
Ni1–N10	2.080(4)	Ni1–N12	2.079(3)	Ni1–N11	2.099(4)	Ni1–N13	2.116(4)
C3–Fe1–C2	89.98(18)	N2–Ni1–N3	89.29(15)	N2[b]–C2–Fe1	173.6(4)	N3–C3–Fe1	177.8(4)
N1–C1–Fe1	177.7(4)	C2–N2–Ni1	160.3(4)	C3–N3–Ni1	173.0(4)	N3–Ni1–N10	95.49(16)
N3–Ni1–N12	177.80(16)	N3–Ni1–N11	88.05(16)	N11–Ni1–N13	163.23(18)		
6							
Fe1–C1	1.913(10)	Fe1–C2	1.938(9)	Fe1–C3	1.894(9)	Fe1–N5	1.964(7)
Fe1–N7	1.917(8)	Fe1–N9	1.958(7)	Ni1–N2[c]	2.040(7)	Ni1–N3	2.108(8)
Ni1–N10	2.059(8)	Ni1–N12	2.086(7)	Ni1–N11	2.102(8)	Ni1–N13	2.102(8)
C3–Fe1–C2	86.7(4)	N2[c]–Ni1–N3	92.0(3)	N2–C2–Fe1	177.0(9)	N3–C3–Fe1	178.5(9)
N1–C1–Fe1	177.2(9)	C2–N2–Ni1[c]	161.6(8)	C3–N3–Ni1	177.2(8)	N3–Ni1–N10	95.3(3)
N3–Ni1–N12	178.1(3)	N3–Ni1–N11	85.4(3)	N11–Ni1–N13	162.5(3)		
7							
Fe1–C1	1.939(4)	Fe1–C2	1.929(4)	Fe1–C3	1.924(4)	Fe1–N5	1.976(3)
Fe1–N7	1.945(3)	Fe1–N9	1.960(3)	Ni1–N2[d]	2.042(3)	Ni1–N3	2.127(4)
Ni1–N10	2.085(3)	Ni1–N12	2.090(4)	Ni1–N11	2.109(3)	Ni1–N13	2.108(3)
C3–Fe1–C2	88.10(17)	N2[d]–Ni1–N3	89.92(14)	N2 –C2–Fe1	174.8(4)	N3–C3–Fe1	177.7(4)
N1–C1–Fe1	178.0(4)	C2–N2–Ni1[d]	164.7(4)	C3–N3–Ni1	175.2(4)	N3–Ni1–N10	94.54(14)
N3–Ni1–N12	177.42(14)	N3–Ni1–N11	86.17(15)	N11–Ni1–N13	163.59(15)		

[a] $-x+2, -y, -z+1$. [b] $-x+1, -y, -z$. [c] $-x+1, -y, -z+1$. [d] $-x+1, -y+2, -z+1$.

$2CH_3OH$ (**7**). Herein, we describe the preparation, structure, and electrochemical and magnetic properties of complexes **1**–**7**.

Results and Discussions

Syntheses and Spectroscopic Studies

In this paper, PhTp {$[PhB(pz)_3]^-$} was synthesized from $PhBCl_2$ and Hpz at room temperature, whereas the reaction for MeTp {$[MeB(pz)_3]^-$} and *i*BuTp {$[iBuB(pz)_3]^-$} required elevated temperatures. $Fe(PhTp)_2$, $Fe(MeTp)_2$, and $Fe(iBuTp)_2$ were isolated as purple solids from the reaction of the relevant tris(pyrazolyl)borates with $FeSO_4$ in deoxygenated water. After reaction with KCN and oxidation by H_2O_2, the tricyanometalate precursors $[(PhTp)Fe(CN)_3]^-$ (**1**), $[(MeTp)Fe(CN)_3]^-$ (**2**), and $[(iBuTp)Fe(CN)_3]^-$ (**3**) were prepared in good yield. Complexes **1**–**3** are soluble in most organic solvents such as methanol, acetonitrile, chloroform, and *N*,*N*-dimethylformamide. The C≡N stretching frequencies are located at 2119 cm^{-1} for **1**, 2120 cm^{-1} for **2**, and 2117 $cm^{-1}$for **3**, which are comparable to those reported in poly(pyrazolyl)borate iron(III) tricyanides $[PPh_4][(Tp)Fe(CN)_3]$ (2121 cm^{-1}),[8a] $[Et_4N][(Tp^*)Fe(CN)_3]$ (2119 cm^{-1}),[17a] and $[Et_4N][(pzTp)Fe(CN)_3]$ (2120 cm^{-1}).[17c]

The incorporation of **1**–**3** into coordinatively unsaturated metal complexes $[Ni(tren)(sol)_2]^{2+}$ or $[Cu(bpy)(sol)_{3-4}]^{2+}$ in methanol (or methanol/water) yielded rectangular clusters **4**–**7**. The bulky coligand (tren or bpy) here precludes the formation of extended arrays. In the IR spectra, two C≡N stretching vibrations are observed (2133 and 2182 cm^{-1} for **4**, 2126 and 2154 cm^{-1} for **5**, 2118 and 2156 cm^{-1} for **6**, and 2120 and 2154 cm^{-1} for **7**), which is consistent with the presence of bridging and terminal cyanide ligands.

Crystal Structures

Selected bond lengths and angles for complexes **1**–**7** are listed in Tables 1 and 2. In the tricyanometalate anions of **1**–**3**, three cyanide ligands in a *fac* arrangement and the tridentate N-donor ligand (PhTp, MeTp, or *i*BuTp) form a distorted octahedral environment around the iron(III) ion (Figure 1). The Fe–C bond lengths in **3** [1.920(3)–1.929(3) Å] are slightly longer than those in **1** [1.901(6)–1.914(7) Å] and **2** [1.909(5)–1.915(5) Å], and all of them are in good agreement with those in low-spin iron(III) tricyanide complexes.[8a,16d,17a] The relevant Fe–N bond lengths and the C–Fe–C and N–Fe–N bond angles are similar for the three tricyanometalate anions (Table 1). The Fe–C≡N angles fall in the range 177.4(6)–179.1(5)° for **1**, 175.8(5)–178.2(4)° for **2**, and 174.9(2)–179.4(3)° for **3**, respectively. The shortest intermolecular Fe···Fe separations are 7.805 Å for **1**, 7.659 Å for **2**, and 7.883 Å for **3**.

The structures of complexes **4**–**7** consist of rectangular units, where Fe^{III} and M^{II} ions (Cu^{II} for **4**, Ni^{II} for **5**–**7**) are located at alternating corners of the rectangle and linked through cyanide bridges. Among various structures and topologies constructed through the cyanide bridges, rectangular clusters are quite simple examples of SMMs, as slow

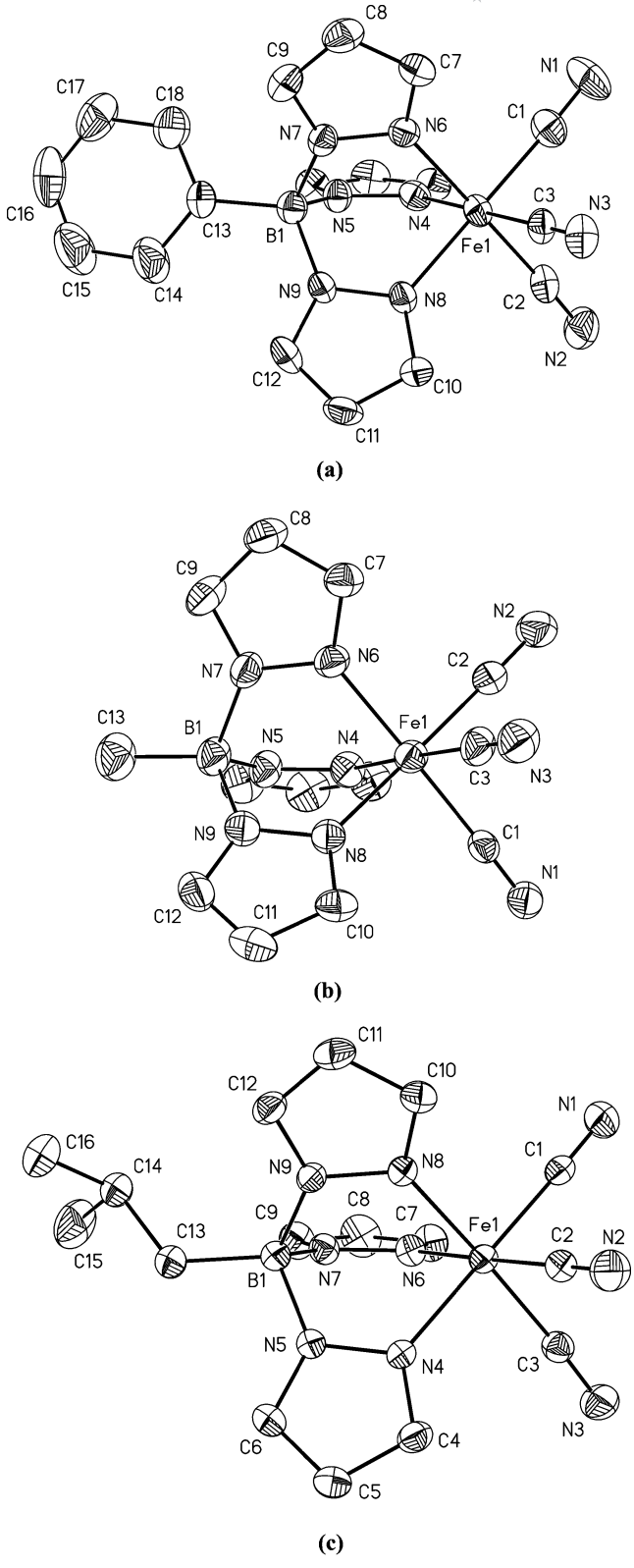

Figure 1. Molecular structures of the anions of complexes **1** (a), **2** (b), and **3** (c). Hydrogen atoms are omitted for clarity (ORTEP, 30% ellipsoids).

relaxation of magnetization was observed in several tetranuclear cyano-bridged clusters,[16c,17a,17d] and they may provide the possibility to study their magnetostructure correlation. In complexes **4**–**7**, each M^{II} ion is linked to two $[(L)Fe(CN)_3]^-$ (L = PhTp for **4**–**5**, MeTp for **6**, and *i*BuTp for **7**) units at the *cis* positions, whereas each octahedral $[(L)Fe(CN)_3]^-$ unit uses its two cyanide units to connect two M^{II} ions, which leaves the third cyanide group free. The bond lengths and angles in the $[(L)Fe(CN)_3]^-$ units in the four compounds are in good agreement with those in the relevant precursors **1**–**3** (Tables 1 and 2).

In complex **4**, the copper atom is six-coordinate as an elongated distorted octahedron of CuN_4O_2 (Figure 2). The equatorial plane is formed by two nitrogen atoms from two cyanide groups and two nitrogen atoms from a bpy ligand; the average length of the Cu–N_{cyano} bond [1.952(4) Å] is slightly shorter than the Cu–N_{bpy} bond length [2.006(9) Å]. The apical positions are occupied by one oxygen atom (O1) of one water molecule and one oxygen atom (O3) of a ClO_4^- anion; the Cu–O bond lengths are 2.370(3) Å (Cu1–O1) and 2.391(3) Å (Cu1–O3). These two labile sites provide the possibility to design larger clusters or polymers with **4** as the precursor. The cyanide bridges connecting the metal centers in **4** are quite close to linearity, and the Fe–C≡N and Cu–N≡C angles vary from 174.8(4) to 177.8(4)°. The intramolecular Fe···Cu distances are 5.003 and 5.014 Å, and the Fe···Fe and Cu···Cu separations are 7.217 and 6.946 Å, respectively. The shortest intermolecular Cu···Cu, Cu···Fe, and Fe···Fe distance are 8.230, 7.679, and 9.810 Å, respectively.

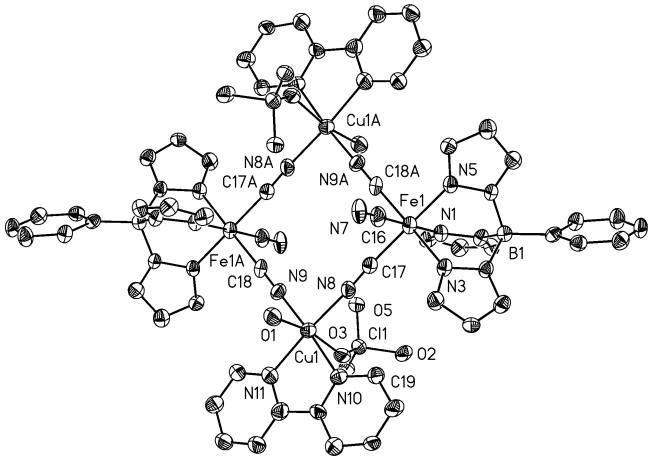

Figure 2. Structure of the rectangular cluster $[(PhTp)Fe(CN)_3Cu(bpy)(H_2O)(ClO_4)]_2$ in complex **4**. Hydrogen atoms are omitted for clarity (ORTEP, 30% ellipsoids).

Complexes **5**–**7** are structurally similar to the $[(Tp)_2(tren)_2Ni_2Fe_2(CN)_6]^{2+}$ cluster reported earlier.[16c] Complexes **5** and **6** crystallize in the triclinic $P\bar{1}$ space group, whereas **7** crystallizes in the monoclinic $P2_1/c$ space group (Figure 3; Supporting Information, Figures S1 and S2). In all three rectangular clusters, the nickel atom has a distorted octahedron coordination geometry constructed by four nitrogen atoms from the tren ligand and two nitrogen atoms from two cyanide bridges. The Ni–N_{tren} bond lengths are distribute in the range 2.059(8)–2.116(4) Å, whereas the Ni–N_{cyano} bond lengths are 2.053(4) and 2.098(4) Å for **5**, 2.040(7) and 2.108(8) Å for **6**, and 2.042(3) and 2.127(4) Å for **7**. The Ni–N≡C angles [160.3(4)–173.0(4)° for **5**, 161.6(8)–177.2(8)° for **6**, and 164.7(4)–175.2(4)° for **7**] deviate somewhat from strict linearity. The differences in the Ni–N≡C angles and Ni–N_{cyano} bond lengths introduce much structural distortion, which results in inequivalent edge lengths of the rectangle in each complex (5.016 and 5.157 Å in **5**, 5.047 and 5.153 Å in **6**, and 5.047 and 5.189 Å in **7**). In **6**, there are weak intermolecular π–π stacking interactions between the adjacent pyrazolyl rings (N4, N5, C4, C5, C6) with a separation of 3.736 Å, which leads to a 1D chain-like structure along the *ab* direction. The chains are further connected through intermolecular hydrogen bonds (N12–H12A···N1 3.298 Å, N11–H11A···N1 3.264 Å, and C4–H4···N1 3.537 Å) to form 2D structures (Supporting Information, Figure S3). However, in **5** and **7** the increasing steric effect around the B atom destroys the intermolecular π–π stacking interactions, and the adjacent clusters are only connected through weak hydrogen bonds (N12–H12B···N1 3.211 Å, N13–H13A···N1 3.263 Å, and C6–H6···N1 3.358 Å for **5** and N12–H12B···N1 3.166 Å, N13–H13C···N1 3.306 Å, and C6–H6···N1 3.567 Å for **7**) to form 1D chain-like structures along the *a* direction (Supporting Information, Figures S4 and S5). The shortest intermolecular Ni···Ni, Ni···Fe, and Fe···Fe distance are 8.706, 6.450, and 8.208 Å for **5**; 8.848, 6.441, and 7.406 Å for **6**; and 8.659, 6.374, and 7.566 Å for **7**, respectively.

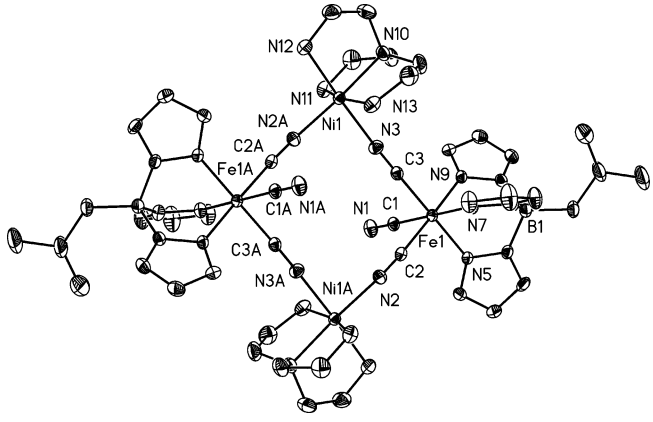

Figure 3. Structure of the rectangular cluster $[(i\text{BuTp})Fe(CN)_3Ni(tren)]_2^{2+}$ in complex **7**. Hydrogen atoms are omitted for clarity (ORTEP, 30% ellipsoids).

Electrochemistry

The electrochemical behavior of mononuclear complexes **1**–**3** and tetranuclear rectangular clusters **5**–**7** was determined by cyclic voltammetry (CV), and the results are summarized in Table 3 and Figures 4 and 5. One quasireversible one-electron redox couple was observed at $E_{1/2}$ = –0.76 V (ΔE_p = 84 mV) for **1**, –0.80 V (ΔE_p = 90 mV) for **2**, and –0.82 V (ΔE_p = 108 mV) for **3** vs. Fc/Fc^+, which is assigned

to the Fe^{2+}/Fe^{3+} process (Figure 4). The observed tendency of $E_{1/2}([(Ph)Fe(CN)_3]^-) > E_{1/2}([(MeTp)Fe(CN)_3]^-) > E_{1/2}$-$[(i\text{BuTp})Fe(CN)_3]^-$) can be rationalized from the electron effect from the organic groups on the B atoms, that is, the stronger donor property of the isobutyl group enriches the electron density but the acceptor property of the phenyl group results in a lower electron density on the Fe^{3+} ion.

Table 3. Cyclic voltammetry data for complexes **1**–**3** and **5**–**7**.[a]

Complex	E_{pa} / V[b]	E_{pc} / V[c]	$E_{1/2}$ / V[d]	ΔE_p / V[e]
1	–0.716	–0.800	–0.76	0.084
2	–0.756	–0.846	–0.80	0.090
3	–0.762	–0.870	–0.82	0.108
5	–0.281	–0.391	–0.34	0.11
	–0.122	–0.270	–0.20	0.148
	0.952	0.867	0.91	0.085
	1.226	1.117	1.17	0.109
6	–0.273	–0.374	–0.32	0.101
	–0.095	–0.266	–0.18	0.171
	0.940	0.840	0.89	0.1
	1.188	1.112	1.15	0.072
7	–0.309	–0.409	–0.36	0.1
	–0.135	–0.299	–0.22	0.164
	0.943	0.852	0.90	0.091
	1.218	1.117	1.17	0.101

[a] Volts vs. Fc/Fc^+, a glassy carbon working electrode, CH_3CN containing 0.1 M Bu_4NClO_4, scan rate of 0.1 V s^{-1}, 25 °C. [b] E_{pa} = oxidative peak potential. [c] E_{pc} = reductive peak potential. [d] $E_{1/2} = (E_{pc} + E_{pa})/2$. [e] $\Delta E_p = E_{pa} - E_{pc}$.

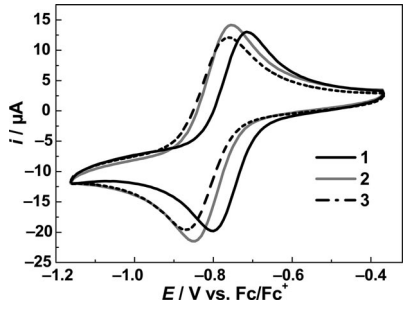

Figure 4. Cyclic voltammograms of complexes **1**–**3** in CH_3CN at a scan rate of 0.1 V s^{-1}.

As shown in Figure 5, the CV of complex **5** (abbreviated as $[Fe^{III}_2Ni^{II}_2]^{2+}$) exhibits four quasireversible waves at –0.34, –0.20, 0.91, and 1.17 V vs. Fc/Fc^+, which are tentatively assigned to four processes:

$$[Fe^{II}_2Ni^{II}_2] \rightleftharpoons [Fe^{III}Fe^{II}Ni^{II}_2]^+ \rightleftharpoons [Fe^{III}_2Ni^{II}_2]^{2+} \rightleftharpoons [Fe^{III}_2Ni^{III}_2]^{4+} \rightleftharpoons [Fe^{III}_2Ni^{III}Ni^{IV}]^{5+}$$

Similarly, complexes **6** and **7** also show two quasireversible iron-centered reduction processes and two quasireversible nickel-centered oxidation processes. These redox potentials can also be compared to those in the complexes containing Fe^{3+} and Ni^{2+} ions.[21] The Fe^{2+}/Fe^{3+} redox waves of complexes **5**–**7** (–0.36 to –0.18 V) are less negative than that of the same reduction process for their precursors **1**–**3** (–0.78 to –0.82 V), which could be attributed to the higher molecular charge, as well as the lower electron density on the Fe^{3+} ion in **5**–**7**.[22] The mixed valence species with grid

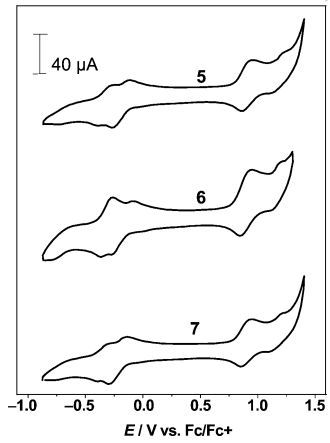

Figure 5. Cyclic voltammograms of complexes **5**–**7** in CH_3CN at a scan rate of 0.1 V s^{-1}.

structure $[Fe^{III}Fe^{II}Ni^{II}_2]^+$ is perhaps an interesting precursor for further studies in molecular electronics, such as quantum dot cellular automata.[23]

Magnetic Properties

Magnetic measurements were performed on polycrystalline samples of complexes **1**–**7**. The magnetic properties of complexes **1**–**3** are shown in Figure S6 (Supporting Information). The values of $\chi_M T$ at 300 K are 0.616 for **1**, 0.651 for **2**, and 0.634 emu K mol^{-1} for **3**, and they decrease slowly as the temperature decreases. This behavior is expected for a distorted low-spin octahedral iron(III) system with spin-orbit coupling of the $^2T_{2g}$ ground term.[24] Below ca. 10 K, $\chi_M T$ decrease smoothly and reaches the minimum values of 0.234 for **1**, 0.351 for **2**, and 0.126 emu K mol^{-1} for **3** at 1.8 K, which can be ascribed to the intermolecular antiferromagnetic interactions.

The temperature dependence of susceptibility for complex **4** was measured in the temperature range of 1.8–300 K. As shown in Figure 6, the $\chi_M T$ value at room temperature is 2.07 emu K mol^{-1}, and it goes up in a mild way in the temperature range 45–300 K, followed by a sharp increase to 4.55 emu K mol^{-1} at 1.8 K, which suggests that there is ferromagnetic coupling between the Fe^{III} and Cu^{II} ions; this is further confirmed by the nearly saturated magnetization value of 3.78 $N\beta$ mol^{-1} under the 7 T magnetic field at 1.8 K (Supporting Information, Figure S7). On the basis of the structure, the Hamiltonian of **4** can be described as: $\hat{H} = -2J[\hat{S}_{Fe1}(\hat{S}_{Cu1} + \hat{S}_{Cu2}) + \hat{S}_{Fe2}(\hat{S}_{Cu1} + \hat{S}_{Cu2})]$, which includes only nearest-neighbor exchange and the Van Vleck expression can be written as Equation (1).

$$\chi_M = \frac{2Ng^2\beta^2}{kT} \times \frac{2 + e^{-2J/kT} + 5e^{2J/kT}}{7 + e^{-4J/kT} + 3e^{-2J/kT} + 5e^{2J/kT}} \quad (1)$$

The best fit between 16 and 300 K gives: $g = 2.308$ and $J = +8.90\ cm^{-1}$ with $R = \Sigma[(\chi_M T)_{calcd} - (\chi_M T)_{obs}]^2/\Sigma[(\chi_M T)^2_{obs}] = 1.5 \times 10^{-3}$, which indicates the existence of ferromagnetic interaction.

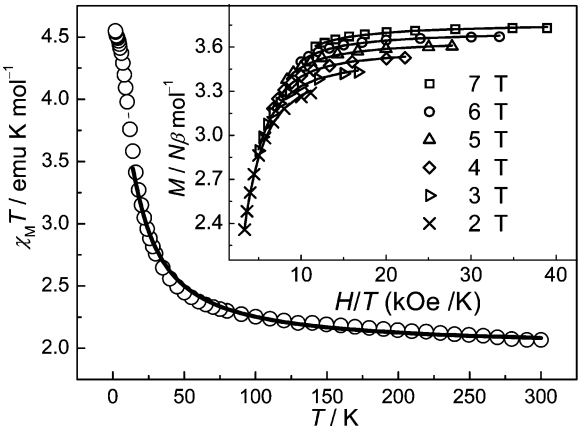

Figure 6. Temperature dependence of $\chi_M T$ for complex **4** recorded under a 2 kOe field. Inset: Reduced magnetization data for **4** at low temperatures. Solid lines represent fits to the data.

The field dependence of the magnetization for **4** at temperatures between 1.8 and 10 K is shown as the M vs. H/T plots in the inset of Figure 6. The nonsuperposition of the isofield lines indicates the presence of significant zero-field splitting. With the spin ground state $S = 2$, fits of the magnetization data with ANISOFIT[6e] afford $D = -4.80$ cm^{-1} with $g = 2.55$. The AC susceptibility studies carried out in the 1.8–10 K range in a 5 Oe oscillating field with frequencies up to 1488 Hz for **4** showed no evidence for magnetic ordering or slow paramagnetic relaxation.

The temperature dependence of susceptibility under 2 kOe for complexes **5**–**7** is displayed in Figure 7. Upon lowering the temperature, the $\chi_M T$ values increase continuously from room temperature values of 3.72, 3.76, and 3.76 emu K mol^{-1} for **5**, **6**, and **7**, respectively, and then reach the maximum values of 6.97, 5.98, and 7.25 emu K mol^{-1} for **5**, **6**, and **7**, respectively, at 9 K for **5** and 10 K for **6** and **7**, after which point they drop sharply and reach values of 2.86, 1.79, and 1.70 emu K mol^{-1} for **5**, **6**, and **7**, respectively, at 1.8 K. This magnetic nature indicates the presence of ferromagnetic coupling between intramolecular Fe^{III} and Ni^{II} ions and is in agreement with the field-dependent magnetization, which shows the unsaturated magnetization values of 5.84, 5.19, and 5.66 $N\beta$ mol^{-1} for **5**, **6**, and **7**, respectively, at 7 T (Supporting Information, Figures S8–S10). A little S shape was observed in the M vs. H plots at 1.8 K for **6** and **7**, which suggests that intermolecular antiferromagnetic interactions at very low temperatures under low field occur. The drop in $\chi_M T$ at very low temperatures could be attributed to the zero-field splitting, weak intermolecular antiferromagnetic interactions, or Zeeman effects. An approximate isotropic Hamiltonian similar to **4** was used to simulate the magnetic susceptibilities:

$$\hat{H} = -2J[\hat{S}_{Fe1}(\hat{S}_{Ni1} + \hat{S}_{Ni2}) + \hat{S}_{Fe2}(\hat{S}_{Ni1} + \hat{S}_{Ni2})]$$

and the Van Vleck expression can be written as Equation (2).

In order to minimize anisotropy effects and intermolecular antiferromagnetic interactions, least-squares fittings of the experimental data were carried out above 9 K (for **5**) and 10 K (for **6** and **7**), which led to $g = 2.284$ and $J = +4.21$ cm^{-1} with $R = 2.4 \times 10^{-3}$ for **5**, $g = 2.305$ and $J = +2.84$ cm^{-1} with $R = 7.7 \times 10^{-3}$ for **6**, and $g = 2.285$ and $J = +5.46$ cm^{-1} with $R = 2.8 \times 10^{-3}$ for **7**.[25]

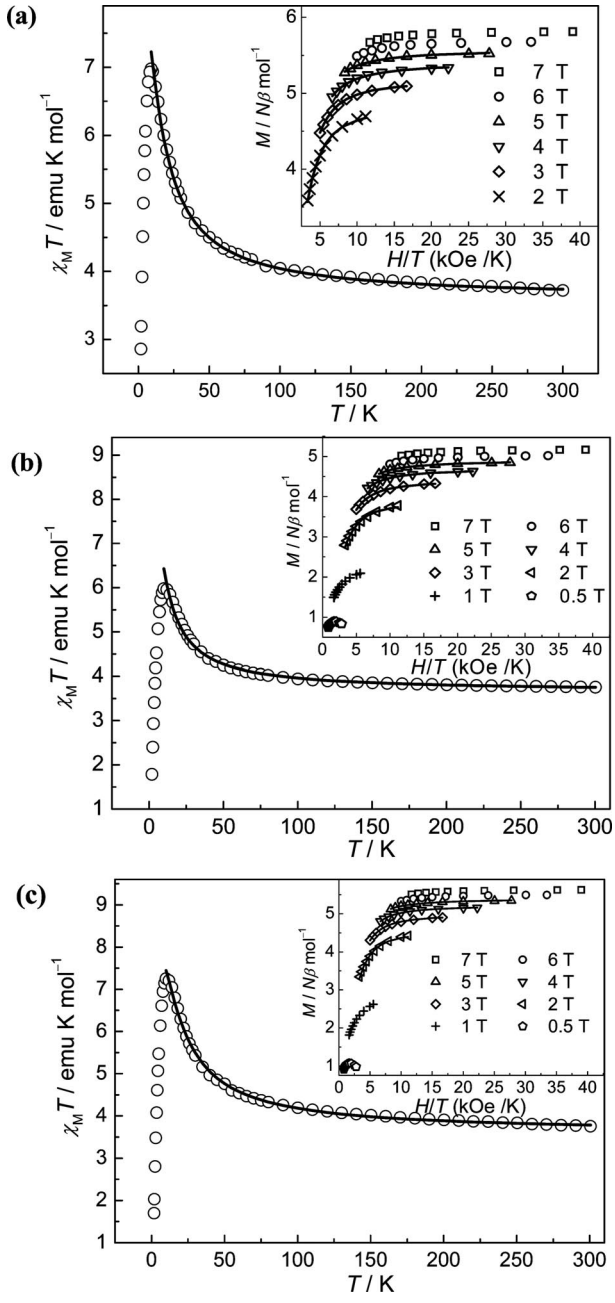

Figure 7. Temperature dependence of $\chi_M T$ for complexes **5** (a), **6** (b), and **7** (c) at 2 kOe. Inset: Reduced magnetization data at low temperatures. Solid lines represent fits to the data.

$$\chi_M = \frac{2Ng^2\beta^2}{kT} \times \frac{7 + e^{-2J/kT} + 10 \times e^{2J/kT} + e^{-6J/kT} + 14 \times e^{4J/kT}}{12 + e^{-4J/kT} + 8 \times e^{-2J/kT} + 5 \times e^{2J/kT} + 3 \times e^{-6J/kT} + 7 \times e^{4J/kT}} \quad (2)$$

The magnetization variations at different magnetic fields were recorded between 1.8 and 6 K (Figure 7, inset). The nonsuperposition of the isofield lines indicates the presence

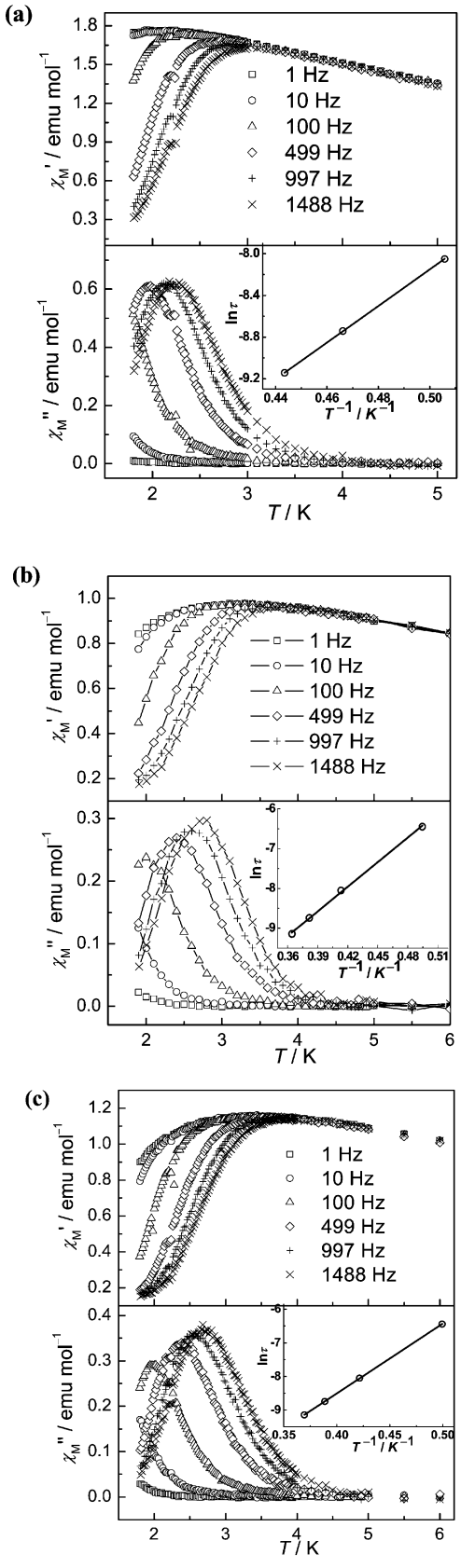

Figure 8. Frequency dependence of the in-phase χ_M' and out-of-phase χ_M'' products vs. T for **5** (a), **6** (b), and **7** (c) in a 5 Oe AC field oscillating at frequencies between 1 and 1488 Hz under a zero DC field. Insert: the Arrhenius fit for the $\ln\tau$ vs. T^{-1} plot.

of significant zero-field splitting. With the magnetic filed of 5 kOe, complexes **6** and **7** show maximum values of magnetization corresponding to the existence of intermolecular interactions.[14c,16c] By considering the relatively small magnitude of exchange parameters, the nonnegligible population of electrons on low-lying excited states should exist, especially under high magnetic field. So, the reduced magnetization data were simulated by using ANISOFIT for $T \leq 6$ K and 50 kOe $\geq H \geq$ 20 kOe to afford D = –3.08 cm^{-1} with g = 2.32 for **5**, D = –3.02 cm^{-1} with g = 2.02 for **6**, and D = –3.25 cm^{-1} with g = 2.27 for **7**.

To investigate the dynamic nature of complexes **5**–**7**, AC magnetic measurements were performed in a 5 Oe AC field oscillating at 1–1488 Hz in the temperature range 1.8–10 K with zero DC field (Figure 8). The obvious frequency-dependent signals in both in-phase (χ_M') and out-of-phase susceptibilities (χ_M'') can be observed below ca. 4 K for **5** and below 5 K for **6** and **7**. The χ_M'' values for a given frequency attain a maximum that shifts to lower temperature upon decreasing the frequency. The χ_M'' peak positions were determined by using fits to Lorentzian lines, and the plots of $\ln\tau$ vs. $1/T$ follow the Arrhenius expression $\ln\tau = U_{eff}/k_BT + \ln\tau_0$, where τ, τ_0, U_{eff}, and k_B represent relaxation time, preexponential factor, relaxation energy barrier, and Boltzmann constant, respectively. Least-squares fittings gave $\tau_0 = 4.5\times10^{-8}$ s for **5**, 6.1×10^{-8} s for **6**, and 5.0×10^{-8} s for **7**, and the effective spin-reversal barriers of U_{eff} = 17.5 K for **5**, 20.6 K for **6**, and 20.8 K for **7**. The χ_M' and χ_M'' signals indicate the existence of slow magnetization relaxation and support the fact that **5**–**7** behave like SMMs.

In complex **6**, the methyl group is less sterically bulky; thus, there is less separation of the rectangle cations and there exists intermolecular π–π stacking interactions (3.736 Å) similar to $[(Tp)_2(tren)_2Ni_2Fe_2(CN)_6]^{2+}$ (3.697 Å).[16c] However, in complexes **5** and **7**, only weak H-bonds connections are observed due to enhancement in the steric effects after the introduction of the Ph or *i*Bu groups. Unfortunately, no direct evidence was detected with regard to the effects on the SMM behavior resulting from the difference in intermolecular interactions.

Conclusions

Three facially tricyanide-containing building blocks **1**–**3** were synthesized and characterized. The incorporation of **1**–**3** into partially blocked salts afforded four rectangular clusters in parallel, $Fe^{III}_2Cu^{II}_2$ (**4**) and $Fe^{III}_2Ni^{II}_2$ (**5**–**7**). The $Fe^{III}_2Ni^{II}_2$ clusters **5**–**7** exhibit two quasireversible iron-centered reduction processes and two quasireversible nickel-centered oxidation processes. Magnetic studies show intramolecular ferromagnetic coupling and appreciable magnetic anisotropy in clusters **4**–**7**. Moreover, **5**–**7** show obvious frequency dependence in the alternating current magnetic susceptibility data, which suggests single-molecule magnet behavior with $\tau_0 = 4.5\times10^{-8}$ s for **5**, 6.1×10^{-8} s for **6**, and 5.0×10^{-8} s for **7**, and the effective spin-reversal barriers of

U_{eff} = 17.5 K for **5**, 20.6 K for **6**, and 20.8 K for **7**. The present results suggest mononuclear compounds **1**–**3** are possible building blocks for assembling new cyanide-bridged heterometallic high-spin clusters with interesting magnetic properties. Our future efforts will focus on the assembly of linear oligomers from expansion of the rectangular SMMs through appropriate linkers to obtain SCMs, as well as controlled assembly of new SMMs.

Experimental Section

Materials and Physical Measurements: All manipulations were carried out under an atmosphere of purified nitrogen by using standard Schlenk techniques. Diethyl ether and toluene were dried by $CaCl_2$ and then distilled from sodium. Methylboronic acid [$MeB(OH)_2$], (2-methylpropyl)boronic acid [iBuB$(OH)_2$], phenyldichloroborane ($PhBCl_2$), $LiAlH_4$, and pyrazole (Hpz) were purchased from Aldrich Chemicals. All other chemicals were reagent grade and used as received. Li[$MeBH_3$]/Li[iBuBH_3] were prepared by using $MeB(OH)_2$/iBuB$(OH)_2$ and $LiAlH_4$ in anhydrous Et_2O as reported previously.[26] Fe$(PhTp)_2$ was synthesized according to modified literature methods.[27] Elemental analyses for C, H, and N were performed with a Perkin–Elmer 240C analyzer. Infrared spectra were recorded with a Vector22 Bruker spectrophotometer as KBr pellets in the 400–4000 cm^{-1} region. Magnetic susceptibility measurements for all crystalline samples were obtained with the use of a Quantum Design MPMS-XL7 SQUID magnetometer in the temperature range 1.8–300 K. The DC measurements were collected up to 70 kOe. Data were corrected for the diamagnetic contribution calculated from Pascal constants.[28] The AC measurements were performed at various frequencies from 1 to 1488 Hz with the AC field amplitude of 5 Oe and no DC field applied. Cyclic voltammetry (CV) experiments were carried out in acetonitrile solution at room temperature with the use of a ZAHNER IM6ex electrochemical working station. A standard three-electrode system with a glassy carbon working electrode, a platinum wire auxiliary electrode, and an Ag/Ag^+ (10 mM $AgNO_3$ in acetonitrile) reference electrode was used. The concentration of the complexes was 1×10^{-3} M for **1**–**3** and 2.5×10^{-4} M for **5**–**7**; tetrabutylammonium perchlorate (0.1 M) was used as the supporting electrolyte. CV was performed at a scan rate of 0.1 $V s^{-1}$. Reported potentials are all referenced to the ferrocene/ferrocenium (Fc/Fc^+) couple, which was used as an internal standard with 0.08 V vs. $Ag/AgNO_3$.

Caution: Although no problems were encountered in this work, $LiAlH_4$ and perchlorate salts are potentially explosive and cyanides are very toxic. Thus, these starting materials should be handled in small quantities and with great care.

Fe$(MeTp)_2$: A solid sample of pyrazole (2.171 g, 31.93 mmol) was added to Li[$MeBH_3$] (0.378 g, 10.56 mmol) in a dry round-bottomed flask under an atmosphere of N_2 with continuous stirring. This mixing caused heat to be generated and H_2 was released. After string for 30 min at room temperature, the mixture was heated at ca. 200 °C for 1.5 h by an air-cooled condenser to a gas meter. The excess pyrazole was removed by sublimation. The product was cooled to room temperature and then dissolved in THF (20 mL), followed by the addition of $FeSO_4 \cdot 7H_2O$ (1.468 g, 5.28 mmol) in deoxygenated water (40 mL). A purple precipitate was immediately formed. After stirring for 1 h, the precipitate was filtered, washed with water and methanol, and purified by recrystallization from CH_2Cl_2. Yield: 1.670 g (62%). IR (KBr): $\tilde{\nu}$ = 2951 (s), 2917 (s), 2850 (m), 1498 (s), 1425 (s), 1410 (vs), 1401 (vs), 1320 (vs), 1301 (vs), 1224 (m), 1101 (vs), 1060 (vs), 1032 (m), 1003 (m), 970 (m), 943 (s), 917 (s), 751 (vs), 710 (s), 759 (s), 620 (m), 550 (m) cm^{-1}.

Fe(iBuTp)$_2$: Fe(iBuTp)$_2$ was prepared as purple microcrystals by using a method similar to that of Fe$(MeTp)_2$, except that Li[iBuBH_3] was used in place of Li[$MeBH_3$]. Yield: 2.101 g (67%). IR (KBr): $\tilde{\nu}$ = 2952 (s), 2922 (s), 2894 (s), 2862 (s), 1499 (s), 1465 (m), 1416 (vs), 1401 (vs), 1366 (m), 1328 (m), 1298 (vs), 1239 (m), 1204 (vs), 1185 (s), 1104 (vs), 1090 (s), 1058 (vs), 1028 (m), 989 (w), 922 (s), 869 (s), 836 (m), 820 (m), 747 (vs), 705 (s), 649 (s), 621 (m), 586 (m) cm^{-1}.

(Bu_4N)[(PhTp)Fe$(CN)_3$]·H_2O (1): A mixture of Fe$(PhTp)_2$ (1.902 g, 3 mmol) and KCN (0.731 g, 11.25 mmol) in 2-propanol (75 mL) was heated at ca. 80 °C under continuous stirring until the color of the suspension changed from purple to yellow. The resulting mixture was cooled to room temperature and concentrated under reduced pressure. The residue was dissolved in boiling water (100 mL) and then filtered hot. The filtrate was cooled to room temperature and Bu_4NBr (0.967 g, 3 mmol) and 30% H_2O_2 (20 mL) were added successively, which caused the precipitation of **1** as a yellow crystalline solid. The crude product was filtered, washed with small portions of water and diethyl ether, and then dried under vacuum at room temperature. Yield: 1.251 g (61%). Yellow plate-shaped crystals of **1** were obtained by slow diffusion of diethyl ether into the solution of **1** in $CHCl_3$. IR (KBr): $\tilde{\nu}$ = 2119 (ν_{CN}) cm^{-1}. $C_{34}H_{52}BFeN_{10}O$ (683.52): calcd. C 59.74, H 7.67, N 20.49; found C 59.67, H 7.79, N 20.32.

(Bu_4N)[(MeTp)Fe$(CN)_3$] (2): Prepared by following the same procedure as that described for **1**. Yield: 0.815 g (45%). X-ray quality crystals of **2** as yellow plates were grown by slow evaporation of the product in H_2O/CH_3OH (1:10). IR (KBr): $\tilde{\nu}$ = 2120 (ν_{CN}) cm^{-1}. $C_{29}H_{48}BFeN_{10}$ (603.43): calcd. C 57.72, H 8.02, N 23.21; found C 57.86, H 8.16, N 23.15.

(Bu_4N)[(iBuTp)Fe$(CN)_3$] (3): Prepared by following the same procedure as that described for **1**. Yield: 1.394 g (72%). Yellow plate-like crystals of **3** were obtained by slow diffusion of diethyl ether into the solution of **3** in $CHCl_3$. IR (KBr): $\tilde{\nu}$ = 2117 (ν_{CN}) cm^{-1}. $C_{32}H_{54}BFeN_{10}$ (645.51): calcd. C 59.54, H 8.43, N 21.70; found C 59.43, H 8.51, N 21.59.

[(PhTp)Fe$(CN)_3$Cu(bpy)(H_2O)(ClO_4)]$_2$·$2H_2O$ (4): To a solution of Cu$(ClO_4)_2 \cdot 6H_2O$ (18.5 mg, 0.05 mmol) in methanol (10 mL) was added a solution of bipy (7.8 mg, 0.05 mmol) in methanol (10 mL), followed by the addition of a solution of (Bu_4N)[(PhTp)Fe$(CN)_3$]·H_2O (34.2 mg, 0.05 mmol) in methanol (5 mL). The resulting solution was concentrated by evaporation in air and then diffused by diethyl ether vapor to afford dark-brown crystals of **4**. Yield: 30.4 mg (78%). IR (KBr): $\tilde{\nu}$ = 2133, 2182 (ν_{CN}) cm^{-1}. $C_{56}H_{52}B_2Cl_2Cu_2Fe_2N_{22}O_{12}$ (1556.5): calcd. C 43.21, H 3.37, N 19.80; found C 43.26, H 3.46, N 19.68.

[(PhTp)Fe$(CN)_3$Ni(tren)]$_2$(ClO_4)$_2$ (5): A methanol solution (10 mL) of Ni$(ClO_4)_2 \cdot 6H_2O$ (18.3 mg, 0.05 mmol) and tren (7.5 mg, 0.05 mmol) was mixed with a solution of (Bu_4N)[(PhTp)Fe$(CN)_3$] (34.2 mg, 0.05 mmol) in methanol (5 mL). Crystals of **5** as orange parallelepipeds were obtained after 1 week upon evaporation of the solvent. Yield: 15.6 mg (43%). IR (KBr): $\tilde{\nu}$ = 2126, 2154 (ν_{CN}) cm^{-1}. $C_{24}H_{32}BClFeN_{13}NiO_4$ (727.45): calcd. C 39.63, H 4.43, N 25.03; found C 39.76, H 4.57, N 24.72.

[(MeTp)Fe$(CN)_3$Ni(tren)]$_2$(ClO_4)$_2$·$2H_2O$ (6): The tren ligand (7.5 mg, 0.05 mmol) was added to a solution of Ni$(ClO_4)_2 \cdot 6H_2O$ (18.3 mg, 0.05 mmol) in CH_3OH/H_2O (3:1, 4 mL), which resulted in the formation of a violaceous solution. Treatment of this mixture with a solution of (Bu_4N)[(MeTp)Fe$(CN)_3$] (30.2 mg, 0.05 mmol)

in methanol (6 mL) afforded an orange solution, which was filtered and left to stand at room temperature. Dark-brown needle-like crystals were obtained after 2 weeks. Yield: 18.8 mg (55%). IR (KBr): $\tilde{\nu}$ = 2118, 2156 (ν_{CN}) cm^{-1}. $C_{19}H_{32}BClFeN_{13}NiO_5$ (683.4): calcd. C 33.40, H 4.72, N 26.64; found C 33.27, H 4.99, N 26.45.

[(*i*BuTp)Fe(CN)$_3$Ni(tren)]$_2$(ClO$_4$)$_2$·2H$_2$O·2CH$_3$OH (7): Red-brown needle-like crystals of **7** were synthesized from $Ni(ClO_4)_2·6H_2O$, tren, and $(Bu_4N)[(iBuTp)Fe(CN)_3]$ by following the same procedure as that described for **5**. Yield: 18.2 mg (48%). IR (KBr): $\tilde{\nu}$ = 2120, 2154 (ν_{CN}) cm^{-1}. $C_{23}H_{42}BClFeN_{13}NiO_6$ (757.52): calcd. C 36.47, H 5.59, N 24.04; found C 36.45, H 5.54, N 23.67.

X-ray Crystallography: The crystal structures of complexes **1**–**7** were determined with a Siemens (Bruker) SMART CCD diffractometer by using monochromated Mo-K_α radiation (λ = 0.71073 Å) at room temperature. Cell parameters were retrieved by using SMART software and refined by using SAINT[29] on all observed reflections. Data were collected by using a narrow-frame method with scan widths of 0.30° in ω and an exposure time of 10 s/frame. The highly redundant data sets were reduced by using SAINT[29] and corrected for Lorentz and polarization effects. Absorption corrections were applied by using SADABS[30] supplied by Bruker. Structures were solved by direct methods with the

Table 4. Crystallographic data for complexes **1**–**3**.

	1	**2**	**3**
Formula	$C_{34}H_{52}BFeN_{10}O$	$C_{29}H_{48}BFeN_{10}$	$C_{32}H_{54}BFeN_{10}$
M_r	683.52	603.43	645.51
Crystal system	monoclinic	monoclinic	monoclinic
Space group	$P2_1/c$	$P2_1/c$	$P2_1/c$
a / Å	15.489(5)	10.003(6)	9.896(3)
b / Å	12.958(5)	13.041(7)	13.143(4)
c / Å	19.804(7)	26.188(14)	27.701(8)
α / °	90	90	90
β / °	101.541(8)	88.212(13)	91.457(5)
γ / °	90	90	90
V / Å^3	3894(2)	3414(3)	3601.4(18)
Z	4	4	4
$\rho_{calcd.}$ / g cm^{-1}	1.166	1.174	1.191
F (000)	1460	1292	1388
T / K	293(2)	293(2)	293(2)
μ / mm^{-1}	0.426	0.475	0.455
Index range	$-18 \le h \le 18$	$-9 \le h \le 11$	$-13 \le h \le 11$
	$-15 \le k \le 15$	$-14 \le k \le 15$	$-17 \le k \le 14$
	$-15 \le l \le 23$	$-23 \le l \le 31$	$-36 \le l \le 36$
Data/restraints/parameters	6825/17/424	5996/7/370	8385/0/397
GOF (F^2)	0.943	0.804	0.892
R_1[a], ωR_2[b] [$I > 2\sigma(I)$]	0.0725, 0.2006	0.0675, 0.1098	0.0519, 0.1206

[a] $R_1 = \Sigma||C| - |F_c||/\Sigma F_o|$. [b] $R_2 = [\Sigma w(F_o^2 - F_c^2)^2/\Sigma w(F_o^2)]^{1/2}$.

Table 5. Crystallographic data for complexes **4**–**7**.

	4	**5**	**6**	**7**
Formula	$C_{56}H_{52}B_2Cl_2Cu_2Fe_2N_{22}O_{12}$	$C_{24}H_{32}BClFeN_{13}NiO_4$	$C_{19}H_{32}BClFeN_{13}NiO_5$	$C_{23}H_{42}BClFeN_{13}NiO_6$
M_r	1556.50	727.45	683.40	757.52
Crystal system	triclinic	triclinic	triclinic	monoclinic
Space group	$P\bar{1}$	$P\bar{1}$	$P\bar{1}$	$P2_1/c$
a / Å	9.810(2)	9.7013(19)	9.6298(17)	9.6999(18)
b / Å	13.202(3)	12.379(2)	11.0552(19)	15.105(3)
c / Å	14.301(4)	14.394(3)	15.103(3)	23.591(4)
α / °	73.015(5)	109.375	68.856(4)	90
β / °	87.899(5)	91.549(4)	85.376(5)	92.725(3)
γ / °	70.838(5)	102.839(4)	87.627(4)	90
V / Å^3	1669.6(7)	1580.4(5)	1494.6(5)	3452.6(11)
Z	1	2	2	4
$\rho_{calcd.}$ / g cm^{-1}	1.548	1.529	1.519	1.457
F (000)	792	750	706	1580
T / K	291(2)	293(2)	293(2)	293(2)
μ / mm^{-1}	1.210	1.193	1.258	1.099
Index range	$-12 \le h \le 12$	$-11 \le h \le 11$	$-11 \le h \le 10$	$-12 \le h \le 11$
	$-15 \le k \le 16$	$-15 \le k \le 12$	$-13 \le k \le 13$	$-19 \le k \le 14$
	$-17 \le l \le 17$	$-17 \le l \le 15$	$-18 \le l \le 15$	$-30 \le l \le 31$
Data/restraints/parameters	6556/0/451	6123/6/415	5742/0/370	8079/0/415
GOF (F^2)	1.034	0.934	0.969	1.089
R_1[a], ωR_2[b] [$I > 2\sigma(I)$]	0.0589, 0.1332	0.0612, 0.1092	0.0960, 0.1359	0.0714, 0.1580

[a] $R_1 = \Sigma||C| - |F_c||/\Sigma F_o|$. [b] $R_2 = [\Sigma w(F_o^2 - F_c^2)^2/\Sigma w(F_o^2)]^{1/2}$.

SHELXL-97 program.[31] The positions of the metal atoms and their first coordination spheres were located from direct-method *E* maps; other non-hydrogen atoms were found by using alternating difference Fourier syntheses and least-squared refinement cycles and, during the final cycles, were refined anisotropically. Hydrogen atoms were placed in calculated position and refined as riding atoms with a uniform value of U_{iso}. Information concerning crystallographic data collection and structure refinement is summarized in Tables 4 and 5. CCDC-663432 (for **1**), -663433 (for **2**), -663434 (for **3**), -663435 (for **4**), -663436 (for **5**), -663437 (for **6**), -663438 (for **7**) contain the supplementary crystallographic data for this paper. These data can be obtained free of charge from The Cambridge Crystallographic Data Centre via www.ccdc.cam.ac.uk/data_request/cif.

Supporting Information (see also the footnote on the first page of this article): Additional structural and magnetic characterization data for the complexes described in this work.

Acknowledgments

This work was supported by the Major State Basic Research Development Program (2006CB806104 and 2007CB925103), the National Science Fund for Distinguished Young Scholars of China (Grant 20725104) and the National Natural Science Foundation of China (Grant 20531040).

[1] a) R. Sessoli, H. L. Tsai, A. R. Schake, S. Wang, J. B. Vincent, K. Folting, D. Gatteschi, G. Christou, D. N. Hendrickson, *J. Am. Chem. Soc.* **1993**, *115*, 1804–1816; b) R. Sessoli, D. Gatteschi, A. Caneschi, M. A. Novak, *Nature* **1993**, *365*, 141–143.

[2] a) D. Gatteschi, R. Sessoli, *Angew. Chem. Int. Ed.* **2003**, *42*, 268–297 and references cited therein; b) L. M. C. Beltran, J. R. Long, *Acc. Chem. Res.* **2005**, *38*, 325–334 and references cited therein.

[3] a) D. A. Garanin, E. M. Chudnovsky, *Phys. Rev. B* **1997**, *56*, 11102–11118; b) G. Christou, D. Gatteschi, D. N. Hendrickson, R. Sessoli, *MRS Bull.* **2000**, *25*, 66–71; c) M. N. Leuenberger, D. Loss, *Nature* **2001**, *410*, 789–793.

[4] a) V. Marvaud, C. Decroix, A. Scuiller, C. Guyard-Duhayon, J. Vaissermann, F. Gonnet, M. Verdaguer, *Chem. Eur. J.* **2003**, *9*, 1677–1691; b) V. Marvaud, C. Decroix, A. Scuiller, F. Tuyèras, C. Guyard-Duhayon, J. Vaissermann, J. Marrot, F. Gonnet, M. Verdaguer, *Chem. Eur. J.* **2003**, *9*, 1692–1705.

[5] a) K. Van Langenberg, S. R. Batten, K. J. Berry, D. C. R. Hockless, B. Moubaraki, K. S. Murray, *Inorg. Chem.* **1997**, *36*, 5006–5015; b) C. P. Berlinguette, J. R. Galán-Mascarós, K. R. Dunbar, *Inorg. Chem.* **2003**, *42*, 3416–3422; c) C. P. Berlinguette, A. Dragulescu-Andrasi, A. Sieber, J. R. Galán-Mascarós, H. U. Güdel, C. Achim, K. R. Dunbar, *J. Am. Chem. Soc.* **2004**, *126*, 6222–6223; d) C. P. Berlinguette, K. R. Dunbar, *Chem. Commun.* **2005**, 2451–2453.

[6] a) J. L. Heinrich, P. A. Berseth, J. R. Long, *Chem. Commun.* **1998**, 1231–1232; b) P. A. Berseth, J. J. Sokol, M. P. Shores, J. L. Heinrich, J. R. Long, *J. Am. Chem. Soc.* **2000**, *122*, 9655–9662; c) J. L. Heinrich, J. J. Sokol, A. G. Hee, J. R. Long, *J. Solid State Chem.* **2001**, *159*, 293–301; d) J. J. Sokol, M. P. Shores, J. R. Long, *Angew. Chem. Int. Ed.* **2001**, *40*, 236–239; e) M. P. Shores, J. J. Sokol, J. R. Long, *J. Am. Chem. Soc.* **2002**, *124*, 2279–2292; f) J. J. Sokol, M. P. Shores, J. R. Long, *Inorg. Chem.* **2002**, *41*, 3052–3054; g) J. Y. Yang, M. P. Shores, J. J. Sokol, J. R. Long, *Inorg. Chem.* **2003**, *42*, 1403–1419.

[7] a) J. N. Rebilly, L. Catala, E. Rivière, R. Guillot, W. Wernsdorfer, T. Mallah, *Inorg. Chem.* **2005**, *44*, 8194–8196; b) J. N. Rebilly, L. Catala, G. Charron, G. Rogez, E. Rivière, R. Guillot, P. Thuéry, A. L. Barra, T. Mallah, *Dalton Trans.* **2006**, 2818–2828.

[8] a) R. Lescouëzec, J. Vaissermann, F. Lloret, M. Julve, M. Verdaguer, *Inorg. Chem.* **2002**, *41*, 5943–5945; b) R. Lescouëzec, L. M. Toma, J. Vaissermann, M. Verdaguer, F. S. Delgado, C. Ruiz-Pérez, F. Lloret, M. Julve, *Coord. Chem. Rev.* **2005**, *249*, 2691–2729.

[9] a) S. Wang, J. L. Zuo, H. C. Zhou, Y. Song, S. Gao, X. Z. You, *Eur. J. Inorg. Chem.* **2004**, 3681–3687; b) Z. G. Gu, Q. F. Yang, W. Liu, Y. Song, Y. Z. Li, J. L. Zuo, X. Z. You, *Inorg. Chem.* **2006**, *45*, 8895–8901.

[10] a) L. Jiang, X. L. Feng, T. B. Lu, S. Gao, *Inorg. Chem.* **2006**, *45*, 5018–5026; b) L. Jiang, H. J. Choi, X. L. Feng, T. B. Lu, J. R. Long, *Inorg. Chem.* **2007**, *46*, 2181–2186.

[11] a) J. Kim, S. Han, I. K. Cho, K. Y. Choi, M. Heu, S. Yoon, B. J. Suh, *Polyhedron* **2004**, *23*, 1333–1339; b) J. Kim, S. Han, K. I. Pokhodnya, J. M. Migliori, J. S. Miller, *Inorg. Chem.* **2005**, *44*, 6983–6988.

[12] a) D. Li, S. Parkin, G. Wang, G. T. Yee, S. M. Holmes, *Inorg. Chem.* **2006**, *45*, 1951–1959; b) D. Li, S. Parkin, G. Wang, G. T. Yee, S. M. Holmes, *Inorg. Chem.* **2006**, *45*, 2773–2775; c) D. Li, S. Parkin, R. Clérac, S. M. Holmes, *Inorg. Chem.* **2006**, *45*, 7569–7571.

[13] a) K. K. Klausmeyer, T. B. Rauchfuss, S. R. Wilson, *Angew. Chem. Int. Ed.* **1998**, *37*, 1694–1696; b) K. K. Klausmeyer, S. R. Wilson, T. B. Rauchfuss, *J. Am. Chem. Soc.* **1999**, *121*, 2705–2711; c) S. C. N. Hsu, M. Ramesh, J. H. Espenson, T. B. Rauchfuss, *Angew. Chem. Int. Ed.* **2003**, *42*, 2663–2666; d) M. Ramesh, T. B. Rauchfuss, *J. Organomet. Chem.* **2004**, *689*, 1425–1430.

[14] a) Z. J. Zhong, H. Seino, Y. Mizobe, M. Hidai, A. Fujishima, S. Ohkoshi, K. Hashimoto, *J. Am. Chem. Soc.* **2000**, *122*, 2952–2953; b) C. P. Berlinguette, D. Vaughn, C. Canãda-Vilalta, J. R. Galán-Mascarós, K. R. Dunbar, *Angew. Chem. Int. Ed.* **2003**, *42*, 1523–1526; c) H. J. Choi, J. J. Sokol, J. R. Long, *Inorg. Chem.* **2004**, *43*, 1606–1608; d) J. M. Herrera, V. Marvaud, M. Verdaguer, J. Marrot, M. Kalisz, C. Mathonière, *Angew. Chem. Int. Ed.* **2004**, *43*, 5468–5471; e) Y. Song, P. Zhang, X. M. Ren, X. F. Shen, Y. Z. Li, X. Z. You, *J. Am. Chem. Soc.* **2005**, *127*, 3708–3709; f) T. Glaser, M. Heidemeier, T. Weyhermüller, R. D. Hoffmann, H. Rupp, P. Müller, *Angew. Chem. Int. Ed.* **2006**, *45*, 6033–6037; g) J. H. Lim, J. H. Yoon, H. C. Kim, C. S. Hong, *Angew. Chem. Int. Ed.* **2006**, *45*, 7424–7426; h) D. E. Freedman, M. V. Bennett, J. R. Long, *Dalton Trans.* **2006**, 2829–2834.

[15] a) J. J. Sokol, A. G. Hee, J. R. Long, *J. Am. Chem. Soc.* **2002**, *124*, 7656–7657; b) E. J. Schelter, A. V. Prosvirin, W. M. Reiff, K. R. Dunbar, *Angew. Chem. Int. Ed.* **2004**, *43*, 4912–4915; c) E. J. Schelter, A. V. Prosvirin, K. R. Dunbar, *J. Am. Chem. Soc.* **2004**, *126*, 15004–15005; d) Z. H. Ni, H. Z. Kou, L. F. Zhang, C. Ge, A. L. Cui, R. J. Wang, Y. Li, O. Sato, *Angew. Chem. Int. Ed.* **2005**, *44*, 7742–7745; e) J. H. Yoon, J. H. Lim, H. C. Kim, C. S. Hong, *Inorg. Chem.* **2006**, *45*, 9613–9615.

[16] a) S. Wang, J. L. Zuo, H. C. Zhou, H. J. Choi, Y. X. Ke, J. R. Long, X. Z. You, *Angew. Chem. Int. Ed.* **2004**, *43*, 5940–5943; b) C. F. Wang, J. L. Zuo, B. M. Bartlett, Y. Song, J. R. Long, X. Z. You, *J. Am. Chem. Soc.* **2006**, *128*, 7162–7163; c) W. Liu, C. F. Wang, Y. Z. Li, J. L. Zuo, X. Z. You, *Inorg. Chem.* **2006**, *45*, 10058–10065; d) Z. G. Gu, W. Liu, Q. F. Yang, X. H. Zhou, J. L. Zuo, X. Z. You, *Inorg. Chem.* **2007**, *46*, 3236–3244.

[17] a) D. Li, S. Parkin, G. Wang, G. T. Yee, A. V. Prosvirin, S. M. Holmes, *Inorg. Chem.* **2005**, *44*, 4903–4905; b) D. F. Li, S. Parkin, G. B. Wang, G. T. Yee, R. Clérac, W. Wernsdorfer, S. M. Holmes, *J. Am. Chem. Soc.* **2006**, *128*, 4214–4215; c) D. F. Li, R. Clérac, S. Parkin, G. B. Wang, G. T. Yee, S. M. Holmes, *Inorg. Chem.* **2006**, *45*, 5251–5253; d) D. F. Li, R. Clérac, G. B. Wang, G. T. Yee, S. M. Holmes, *Eur. J. Inorg. Chem.* **2007**, 1341–1346.

[18] a) K. R. Dunbar, R. A. Heintz, *Prog. Inorg. Chem.* **1997**, *45*, 283–391; b) H. Weihe, H. U. Güdel, *Comments Inorg. Chem.* **2000**, *22*, 75–103; c) J. S. Miller, *MRS. Bull.* **2000**, *25*, 60–64.

[19] a) S. Wang, J. L. Zuo, S. Gao, Y. Song, H. C. Zhou, Y. Z. Zhang, X. Z. You, *J. Am. Chem. Soc.* **2004**, *126*, 8900–8901; b) H. R. Wen, C. F. Wang, Y. Song, S. Gao, J. L. Zuo, X. Z. You, *Inorg. Chem.* **2006**, *45*, 8942–8949.
[20] a) A. Palii, S. M. Ostrovsky, S. I. Klokishner, B. S. Tsukerblat, K. R. Dunbar, *ChemPhysChem* **2006**, *7*, 871–879; b) K. Park, S. M. Holmes, *Phys. Rev. B* **2006**, *74*, 224440.
[21] a) P. Chaudhuri, M. Winter, B. P. C. D. Védova, P. Fleischhauer, W. Haase, U. Flörke, H. J. Haupt, *Inorg. Chem.* **1991**, *30*, 4777–4783; b) D. Burdinski, F. Birkelbach, T. Weyhermüller, U. Flörke, H. J. Haupt, M. Lengen, A. X. Trautwein, E. Bill, K. Wieghardt, P. Chaudhuri, *Inorg. Chem.* **1998**, *37*, 1009–1020.
[22] H. Oshio, O. Tamada, H. Onodera, T. Ito, T. Ikoma, S. Tero-Kubota, *Inorg. Chem.* **1999**, *38*, 5686–5689.
[23] M. Ruben, J. Rojo, F. J. Romero-Salguero, L. H. Uppadine, J. M. Lehn, *Angew. Chem. Int. Ed.* **2004**, *43*, 3644–3662.
[24] a) L. L. Martin, R. L. Martin, K. S. Murray, A. M. Sargeson, *Inorg. Chem.* **1990**, *29*, 1387–1394; b) R. Lescouëzec, F. Lloret, M. Julve, J. Vaissermann, M. Verdaguer, R. Llusar, S. Uriel, *Inorg. Chem.* **2001**, *40*, 2065 –2072; c) L. M. Toma, R. Lescouëzec, J. Pasán, C. Ruiz-Pérez, J. Vaissermann, J. Cano, R. Carrasco, W. Wernsdorfer, F. Lloret, M. Julve, *J. Am. Chem. Soc.* **2006**, *128*, 4842–4853.
[25] The experimental data were also fitted including the intermolecular interactions (z*J'*) within a mean-field approximation. However, the simulations are very rough. See Figure S11 in the Supporting Information.
[26] a) B. Singaram, T. E. Cole, H. C. Brown, *Organometallics* **1984**, *3*, 774–777; b) H. V. R. Dias, X. Wang, *Polyhedron* **2004**, *23*, 2533–2539.
[27] a) S. Trofimenko, *J. Am. Chem. Soc.* **1967**, *89*, 6288–6294; b) Y. Sohrin, H. Kokusen, M. Matsui, *Inorg. Chem.* **1995**, *34*, 3928–3934.
[28] L. N. Mulay, E. A. Boudreaux, *Theory and Applications of Molecular Diamagnetism*, John Wiley & Sons Inc., New York, **1976**.
[29] *SAINT-Plus*, version 6.02, Bruker Analytical X-ray System, Madison, WI, **1999**.
[30] G. M. Sheldrick, *SADABS*s: *An Empirical Absorption Correction Program*, Bruker Analytical X-ray Systems, Madison, WI, **1996**.
[31] G. M. Sheldrick, *SHELXTL-97*, University of Göttingen, Germany, **1997**.

Received: October 13, 2007
Published Online: January 2, 2008

